

Resonant X-ray Scattering Study of Charge Density Wave Correlations in $\text{YBa}_2\text{Cu}_3\text{O}_{6+x}$

S. Blanco-Canosa,^{1,2} A. Frano,^{1,2} E. Schierle,² J. Porras,¹ T. Loew,¹
M. Minola,¹ M. Bluschke,¹ E. Weschke,² B. Keimer,^{1,*} and M. Le Tacon,^{1,†}

¹Max-Planck-Institut für Festkörperforschung, Heisenbergstr. 1, D-70569 Stuttgart, Germany

²Helmholtz-Zentrum Berlin für Materialien und Energie,
Albert-Einstein-Strasse 15, D-12489 Berlin, Germany

(Dated: September 22, 2022)

We report the results a comprehensive study of charge density wave (CDW) correlations in untwinned $\text{YBa}_2\text{Cu}_3\text{O}_{6+x}$ single crystals with $0.4 \leq x \leq 0.99$ using $\text{Cu-}L_3$ edge resonant x-ray scattering (RXS). Evidence of CDW formation is found for $0.45 \leq x \leq 0.93$ (hole doping levels $0.086 \lesssim p \lesssim 0.163$), but not for samples with $x \leq 0.44$ ($p \lesssim 0.084$) that exhibit incommensurate spin-density-wave order, and in slightly overdoped samples with $x = 0.99$ ($p \sim 0.19$). This suggests the presence of two proximate zero-temperature CDW critical points at $p_{c1} \sim 0.08$ and $p_{c2} \sim 0.18$. Remarkably, p_{c2} is the doping level that is optimal for superconductivity. The CDW reflections are observed at incommensurate in-plane wave vectors $(\delta_a, 0)$ and $(0, \delta_b)$ with $\delta_a \lesssim \delta_b$. Both δ_a and δ_b decrease linearly with increasing doping, in agreement with recent reports on Bi-based high- T_c superconductors, but in sharp contrast to the behavior of the $\text{La}_{2-x}(\text{Ba},\text{Sr})_x\text{CuO}_4$ family. The CDW intensity and correlation length exhibit maxima at $p \sim 0.12$, coincident with a plateau in the superconducting transition temperature T_c . The onset temperature of the CDW reflections depends non-monotonically on p , with a maximum of ~ 160 K for $p \sim 0.12$. The RXS reflections exhibit a uniaxial intensity anisotropy. Whereas in strongly underdoped samples the reflections at $(\delta_a, 0)$ are much weaker than those at $(0, \delta_b)$, the anisotropy is minimal for $p \sim 0.12$, and reversed close to optimal doping. We further observe a depression of CDW correlations upon cooling below T_c , and (for samples with $p \geq 0.09$) an enhancement of the signal when an external magnetic field up to 6 T is applied in the superconducting state. For samples with $p \sim 0.08$, where prior work has revealed a field-enhancement of incommensurate magnetic order, the RXS signal is field-independent. This supports a previously suggested scenario in which incommensurate charge and spin orders compete against each other, in addition to individually competing against superconductivity (Blanco-Canosa *et al.*, Phys. Rev. Lett. **110**, 187001 (2013)). We discuss the relationship of these results to prior observations of “stripe” order in $\text{La}_{2-x}(\text{Ba},\text{Sr})_x\text{CuO}_4$, the “pseudogap” phenomenon, superconducting fluctuations, and quantum oscillations, as well as their implications for the mechanism of high-temperature superconductivity.

PACS numbers: 74.20.Rp, 74.25.Gz, 74.25.Kc, 74.72.Bk

I. INTRODUCTION

The interplay between spin and charge degrees of freedom in materials with strongly correlated electrons generates complex phase diagram in which the balance between various competing phases can be tuned through parameters such as temperature, doping, pressure, and magnetic field. In the layered cuprates, removing electrons from the undoped, Mott-insulating CuO_2 planes suppresses long-range antiferromagnetic order and gives rise to high temperature superconductivity¹. For large concentrations of holes, p , per Cu ion, superconductivity disappears, and the emerging metallic state is amenable to a description by the Fermi-liquid theory. In the underdoped regime bridging the Mott-insulating and the fully developed superconducting states, however, the physical properties of the cuprates indicate the breakdown of conventional Fermi-liquid models.²

Research on the origin of the “non-Fermi liquid” behavior of the underdoped cuprates has uncovered evidence charge-ordering phenomena in the CuO_2 planes^{3–36}. The initial experimental evidence for charge

order was found in the “214” family [$\text{La}_{2-x}\text{Ba}_x\text{CuO}_4$ and $\text{La}_{1.8-x}(\text{Nd},\text{Eu})_{0.2}\text{Sr}_x\text{CuO}_4$] where it was found to be intimately linked to doping-induced incommensurate spin correlations^{3–8}. For $p \sim 1/8$, uniaxial “stripe” domains with approximately commensurate periodicity (~ 4 lattice constants a for charge, and $\sim 8a$ for spin degrees of freedom) and correlation lengths up to several tens of unit cells suppress the development of superconductivity. The influence of static or fluctuating stripe domains on the fermiology of underdoped cuprates has been extensively discussed^{9,37,38}. However, disorder introduced by the randomly placed Sr donor sites, which has thus far precluded the observation of coherent quantum transport phenomena in the 214 system, remains a significant impediment to a full understanding of this key issue.

In $\text{YBa}_2\text{Cu}_3\text{O}_{6+x}$ (hereafter YBCO_{6+x}) and related “123” compounds, doping-induced disorder is significantly reduced³⁹ because the oxygen dopant atoms are arranged in CuO chains stacked between the CuO_2 layers. Depending on the oxygen content, x , the chains form different ordering patterns ranging from the “ortho-II” structure for $x \sim 0.5$, where full and empty chains alter-

nate, to the “ortho-I” structure for $x \sim 0.99$, where all oxygen positions in the CuO chain layer are occupied.⁴⁰ In ortho-II ordered YBCO_{6+x} crystals with $x \sim 0.5$ ($p \sim 0.1$), quantum oscillations have been observed in both transport and thermodynamic experiments in magnetic fields sufficient to obliterate superconducting long-range order^{35,36,41–43}. Nuclear magnetic resonance (NMR) experiments motivated in part by these results revealed a magnetic-field-induced modulation of the charge density in underdoped YBCO_{6+x}, without any signature of static magnetism^{20,21}.

Subsequent resonant^{22–25} and non-resonant^{26–28} x-ray scattering experiments demonstrated static²⁹ CDW order with domain sizes up to ~ 20 unit cells even in the absence of magnetic fields. The temperature and magnetic field dependence of the x-ray intensity implies a competition between CDW formation and superconductivity in YBCO_{6+x}. The x-ray studies determined the periodicity of the charge-ordered state, which turned out to be incommensurate with the underlying lattice. The CDW wavevector is along the Cu-O bond directions in the CuO₂ planes, with $q_{CDW} = (\delta_a, 0, 0.5)$, $(0, \delta_b, 0.5)$ and $\delta_a \lesssim \delta_b \sim 0.3$. [We quote the wavevector coordinates $q = (h, k, l)$ in reciprocal lattice units (r.l.u.) based on an orthorhombic unit cell where the c -axis is perpendicular to the CuO₂ planes, and the b -axis is parallel to the CuO chains.], and is consistent with model calculations that attribute the small Fermi surface pockets seen in the quantum oscillation experiments to a Fermi-surface reconstruction triggered by bi-axial CDW order.⁴⁴

Resonant x-ray scattering (RXS) experiments have also revealed evidence of CDW order in Bi₂Sr₂CuO_{6+δ} and Bi₂Sr₂CaCu₂O_{8+δ},^{32,33} in good agreement with prior results of surface-sensitive scanning tunneling spectroscopy measurements.^{14–19} Together with recent data on HgBa₂CuO_{4+δ} that also indicate CDW correlations,⁴⁵ these observations demonstrate that the CDW is a generic feature of the underdoped cuprates. An important open question is the relationship between the “pseudogap”, another phenomenon that is ubiquitous in underdoped cuprates, and the gap associated with CDW formation. A comparative RXS and angle-resolved photoemission spectroscopy (ARPES) study of Bi₂Sr₂CuO_{6+δ} has begun to address this question by showing that the CDW wavevector matches the distance between the tips of the ungapped segments (“Fermi arcs”) of the quasi-two-dimensional Fermi surface³².

Most of these studies (except those on the 214 system) have been carried out over a limited range of doping levels. In YBCO_{6+x}, CDW correlations have been observed between $p \sim 0.1$ ^{22,24,25,27} and $p \sim 0.13$ ²³, where static magnetism is absent and the magnetic response is fully gapped^{46,47}. In this range of p , the incommensurability δ decreases with increasing p , as expected based on models that link the CDW to the Fermi surface, but in contrast to the 214 materials which exhibit the opposite trend. For ortho-II ordered YBCO_{6+x} with $p \sim 0.1$, the charge modulation is weaker than the one observed at

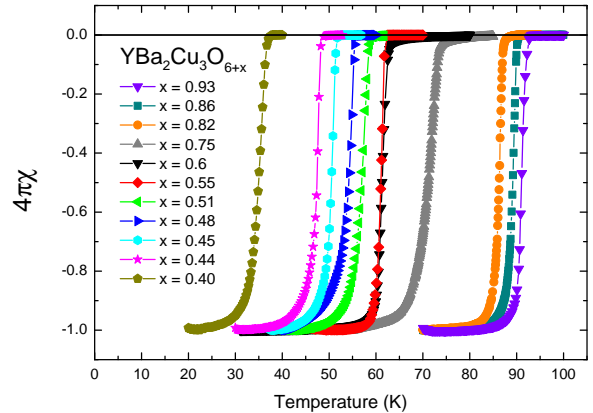


FIG. 1: (Color online) Magnetization curves of the set of samples investigated here.

higher doping levels, and the CDW amplitude along the H -direction of reciprocal space is considerably lower than along K ^{24,27}. For lower p , static incommensurate magnetic short-range order with propagation vector along H has been observed^{48–50}, but evidence for a modulation of the charge density has not been reported²².

In order to provide further insight into the relationship between CDW correlations, quantum oscillations, the pseudogap, and superconductivity, we have undertaken a comprehensive RXS study of the doping, temperature, and magnetic field dependence of the CDW in YBCO_{6+x} covering doping levels ranging from $p \sim 0.07$ ($x = 0.4$) to $p \sim 0.19$ ($x = 0.99$). The results complement and extend prior RXS work in a more limited range of p . Important new results include the linear doping dependence of q_{CDW} over the entire range of p where CDW are observable by RXS, the systematic evolution of the in-plane anisotropy of the CDW, and the discovery of CDW correlations up to (but not beyond) optimal doping ($p \sim 0.18$). The CDW quantum critical point near optimal doping indicated by these results may have important implications for the mechanism of high-temperature superconductivity.

II. EXPERIMENTAL DETAILS

A. Single crystals

YBCO_{6+x} single crystals were synthesized using a flux method as described in previous reports⁵¹. In addition to the crystals with oxygen contents $x = 0.55$ and 0.6 previously studied by RXS^{22,24,25}, we present results obtained on single crystals with both lower x ranging from 0.40 ($p \sim 0.07$) to 0.51 ($p \sim 0.1$), and higher x between 0.75 ($p \sim 0.14$) and 0.99 ($p \sim 0.19$). The oxygen content was controlled by annealing under well-defined oxygen partial pressure, and the c -axis lattice parameters were used to

Sample	Structure	T_c (K)	c -axis (Å)	p
YBCO _{6.40}	O-II	35	11.771	0.072
YBCO _{6.44}	O-II	47.4	11.760	0.084
YBCO _{6.45}	O-II	50.5	11.758	0.086
YBCO _{6.48}	O-II	54.2	11.752	0.092
YBCO _{6.51}	O-II	57	11.745	0.099
YBCO _{6.55}	O-II	61	11.731	0.114
YBCO _{6.6}	O-VIII	61	11.72	0.12
YBCO _{6.75}	O-III	71	11.7156	0.134
YBCO _{6.82}	O-III	86.5	11.706	0.148
YBCO _{6.86}	O-I	89	11.703	0.152
YBCO _{6.93}	O-I	91	11.6969	0.163
YBCO _{6.99}	O-I	90	11.6835	0.189

TABLE I: List of the YBa₂Cu₃O_{6+x} crystals investigated by RXS. The structural arrangement of oxygen donor atoms is labeled O-II for ortho-II, etc.^{40,54} The superconducting transition temperature T_c was determined by magnetometry. The room temperature out-of-plane lattice parameter, c , was determined by hard x-ray diffraction. From this value, the hole doping level p per planar Cu ion was extracted following Ref. 53.

determine the hole-doping levels^{52,53}. All samples were mechanically detwinned by heating under uniaxial stress. T_c is quoted as the midpoint of the transition determined from magnetization measurements performed in a VSM SQUID magnetometer (Fig. 1).

Some of the samples listed in Table I exhibit an ortho-II type of oxygen superstructure comprising alternating full and empty CuO chains. The correlation length for this order decreases along with the oxygen concentration. In previous hard x-ray diffraction work on the YBCO_{6.55} single crystal, it has been estimated as ~ 100 Å²⁴. Due to an unfavorable scattering geometry, it is hard to determine this correlation length directly from soft x-ray scattering measurements on an absolute scale. A qualitative picture can, however, be drawn from the doping dependence of the width of the superstructure peak measured at the L₃ resonance of chain Cu at $q = (0.5, 0, l)$; note that in a rocking scan that covers the range 0.45-0.55 for h , l varies between ~ 1 and 0.5 (see Section II B). The ortho-II domain size estimated on the basis of these measurements indeed increases by a factor of ~ 3 between YBCO_{6.55} and YBCO_{6.40} (Fig. 2), in good agreement with previous studies^{40,54}. The YBCO_{6.6} crystal showed ortho-VIII correlations, and ortho-III correlations were observed in the crystals with higher oxygen contents, again in agreement with prior work^{40,54}. Crystals with $x \geq 0.79$ only showed ortho-I correlations.

B. Resonant x-ray scattering

In this section, we recall some basis features of resonant soft x-ray scattering (RXS). For more details, see the recent review in Ref. 55). The resonant scattering intensity $I(\omega)$ depends on the incoming photon energy,

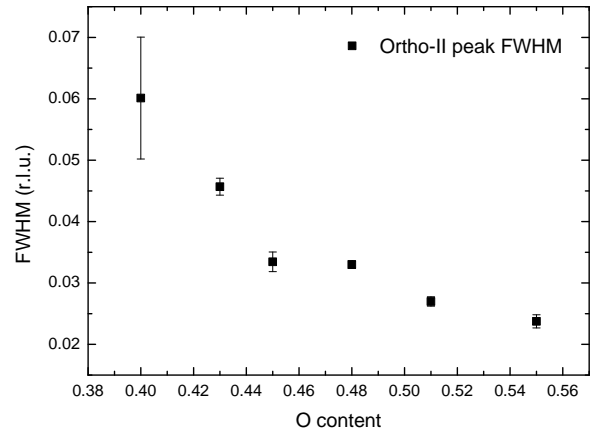


FIG. 2: (Color online) Full-width-at-half-maximum of the ortho-II superstructure peak measured at $q = (0.5, 0, l)$ with photon energy tuned to the L₃ absorption edge of the chain Cu atoms as a function of the oxygen content x in YBCO_{6+x}.

$\hbar\omega$, and can be described as

$$I(\omega) = \left| \sum_n e^{iq \cdot R_n} (\epsilon'^* \cdot F_n(\omega) \cdot \epsilon) \right|^2 \quad (1)$$

where q denotes the scattering vector, R_n is the position of the n^{th} atom, ϵ (ϵ') is the incoming (outgoing) polarization, and $F_n(\omega)$ is the energy dependent scattering tensor (also known as form factor) for each atomic species. F_n reflects both charge and magnetic degrees of freedom.

By tuning the incident photon energy to a specific x-ray absorption edge, the atomic structure factor F_n is strongly enhanced. RXS experiments are therefore directly sensitive to the valence electron states, as compared to other techniques such as nuclear neutron or hard x-ray scattering which probe the lattice displacements induced by the modulation of the valence electron density.

Zero-field RXS measurements were performed in the UHV diffractometer at the UE46-PGM1 beamline of the Helmholtz-Zentrum Berlin at BESSY-II, with incoming light polarization perpendicular to the scattering plane. Magnetic field dependent measurements (up to $H = 6$ T) were performed at the same beamline. The field was applied at an angle of 11.5° to the c -axis, nearly perpendicular to the CuO₂ planes. The data were not corrected for self-absorption. The background measured in the magnet chamber was found to be independent of the applied magnetic field.

The crystals were aligned with the CuO₂ planes perpendicular to the scattering plane. Close to the CDW peak position at $q = (0, \delta_b, l)$, this geometry restricts the l -values we can reach at the Cu-L₃ edge to $1.35 \leq l \leq 1.45$, which is close to the half-integer l -value that maximizes the scattering intensity of the CDW peak^{26,29}.

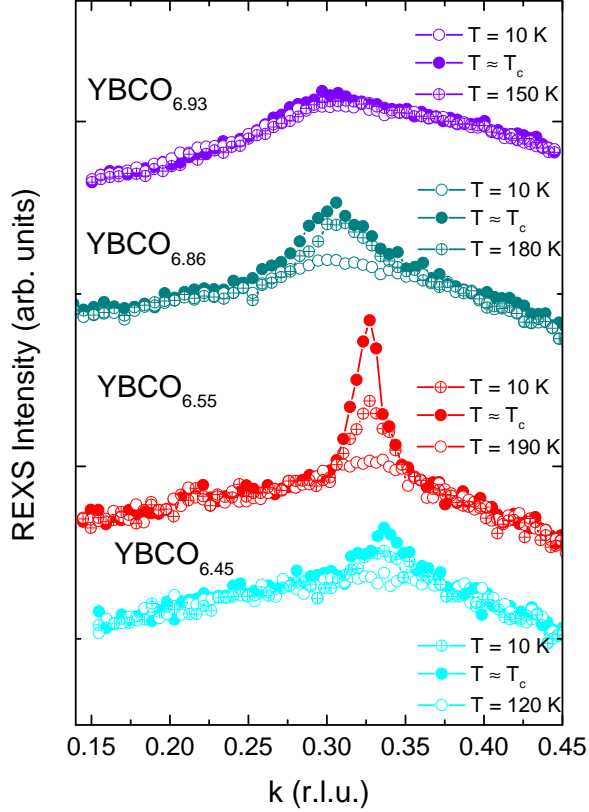


FIG. 3: (Color online) Raw data measured along the (0,1,0) direction for $\text{YBa}_2\text{Cu}_3\text{O}_{6+x}$ samples with $x = 0.45, 0.55, 0.86,$ and 0.93 close to their respective T_c (full symbols) and above the onset of the CDW signal (empty symbols).

III. RESULTS

A. Doping dependence

Figure 3 presents raw data taken on different YBCO_{6+x} crystals at their respective T_c , together with background scans at higher temperatures. Many of our key results are already apparent in the unprocessed scans. As reported in Ref. 24, a superstructure peak associated with CDW correlations is observed in the RXS spectra of $\text{YBCO}_{6.55}$ at $q_{\text{CDW}} = (0, 0.326, l)$. With both increasing and decreasing oxygen content, CDW peaks remain clearly visible on top a temperature independent background, which was determined by measuring the RXS signal at higher temperatures above which it remains temperature independent. This onset temperature ranges from ~ 110 to 160 K depending on the doping level (see below). Note that an extremely broad, temperature independent peak centered at approximately the same position remains visible even above the onset temperature determined in this way.

Special care was taken to perform all the measurements

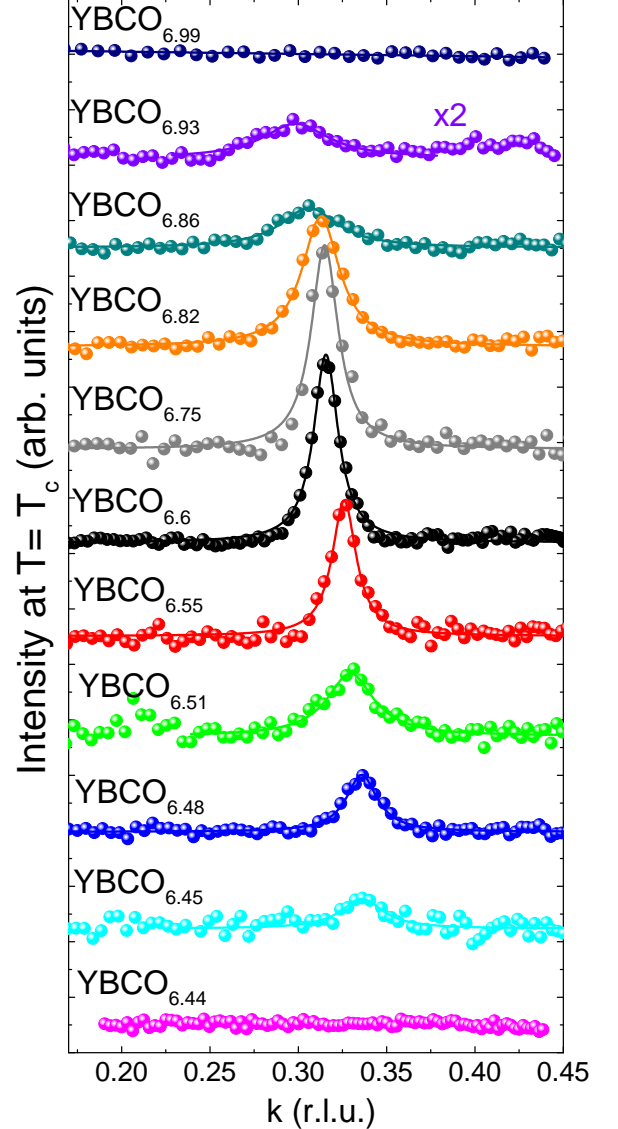


FIG. 4: (Color online) Background-subtracted RXS intensity measured along the (0, 1, 0) direction for a set of $\text{YBa}_2\text{Cu}_3\text{O}_{6+x}$ samples with $0.44 < x < 0.99$. Solid lines are the results of fits to Lorentzian profiles.

presented in this paper under comparable experimental conditions. Although quantitative comparisons of absolute RXS intensities from sample to sample remain difficult, especially since details of the oxygen order can significantly affect the intensity of the CDW peak⁵⁶, a pronounced intensity maximum for $p \sim 0.12$ can be clearly identified on a qualitative level. The temperature, magnetic field, and wave vector dependence of the RXS intensity for individual samples as well as the p -dependence of the peak position and width are unaffected by sample-to-sample intensity variations and can be accurately extracted from the data in Fig. 3.

Figure 4 displays background-subtracted data obtained for representative samples with oxygen concentrations ranging from $x = 0.44$ to 0.99 at their respective T_c . Signatures of CDW formation are not found for oxygen contents lower than $x = 0.45$ ($p = 0.086$) and in fully oxygenated $\text{YBCO}_{6.99}$ ($p = 0.189$). At all other doping levels, temperature dependent CDW correlations can be identified, with a pronounced intensity maximum for $p \sim 0.12$. We will henceforth refer to the doping range $0.08 \lesssim p \lesssim 0.18$ where CDW correlations are observable by RXS as the “CDW stability range”. Since the CDW correlation length always remains finite, however, these data do not imply thermodynamic stability of the CDW.

B. Anisotropy

So far, we have focused on the CDW peak along the $(0,1,0)$ (k)-direction. As already noted in Refs. 24,27, the CDW is highly anisotropic in the ortho-II ordered sample $\text{YBCO}_{6.55}$, where the intensity is strongly reduced along the $(1,0,0)$ (h)-direction. In the samples with $x < 0.55$ investigated here, the CDW peak is only observed along k . This is illustrated in Fig. 5 where background-subtracted data at $T = T_c$ are shown along both h and k . At higher doping levels, the CDW is much more isotropic, as previously reported in $\text{YBCO}_{6.6}$ 22 and $\text{YBCO}_{6.75}$ 23. For $x = 0.86$, we now find that the peak along h is slightly more intense than the one along k , so that the anisotropy is reversed compared to the samples with $x < 0.6$.

Figure 5 also shows that at each doping level where the signatures of charge modulations are seen in both directions, the incommensurability along h is always slightly smaller than along k , as pointed out in Refs. 24,27 for a more limited set of samples. In order to extract the peak width and position, the data of Fig. 4 were fitted to Lorentzian profiles. Figure 6a shows a summary plot of the doping dependence of the incommensurability determined in this way over the entire CDW stability range. Both δ_a and δ_b decrease linearly with increasing doping. This behavior contrasts markedly with the one in the 214 materials shown for comparison in Fig. 6b, where δ first increases with increasing p and then saturates for $p \sim 1/8$.

Figure 7a displays the doping dependence of the Lorentzian full-width-at-half-maximum (FWHM) of the CDW peak at T_c in both directions. The correlation length ξ extracted from these data (Fig. 7b) reaches a maximum of ~ 75 Å (about 20 lattice spacings) for $p \sim 0.12$, mirroring the amplitude maximum inferred from the raw data in Fig. 3. Near the end points of the CDW stability range, $\xi \sim 30$ Å (about 8 lattice spacings), comparable to the CDW correlation lengths observed in $\text{Bi}_2\text{Sr}_2\text{CuO}_{6+\delta}$, $\text{Bi}_2\text{Sr}_2\text{CaCu}_2\text{O}_{8+\delta}$, and $\text{HgBa}_2\text{CuO}_{4+\delta}$. For the samples with the largest ξ , the peak widths in the h - and k -directions differ by up to $\sim 50\%$, which translates into a highly anisotropic correlation volume in the CuO_2 planes.

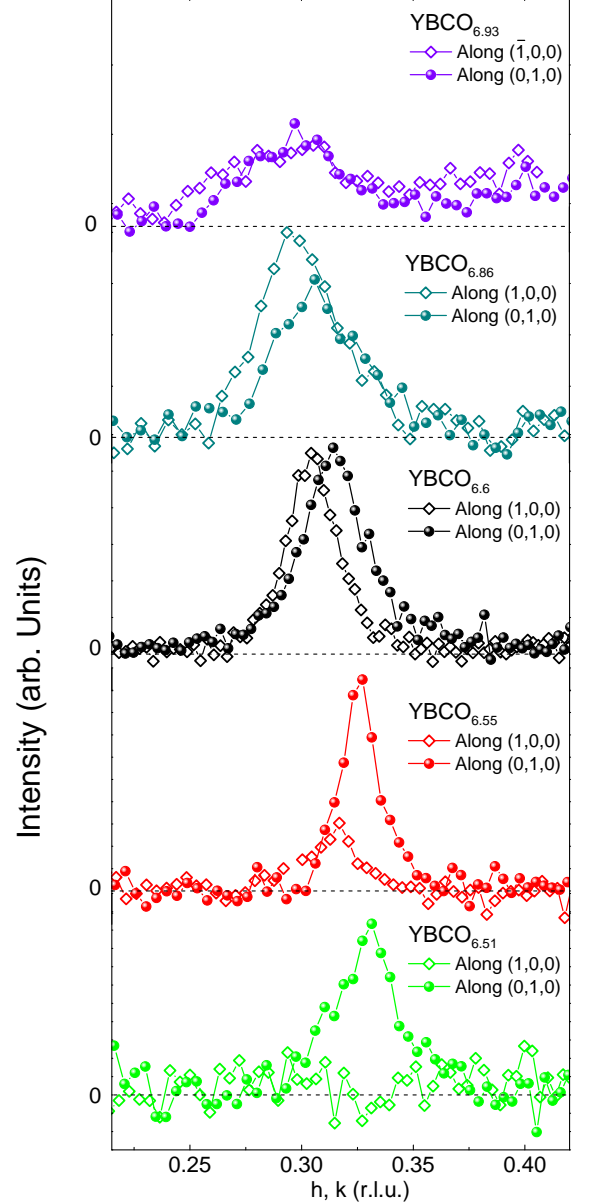


FIG. 5: (Color online) In-plane anisotropy of the RXS signal in $\text{YBa}_2\text{Cu}_3\text{O}_{6.86}$, $\text{YBa}_2\text{Cu}_3\text{O}_{6.6}$, $\text{YBa}_2\text{Cu}_3\text{O}_{6.55}$, and $\text{YBa}_2\text{Cu}_3\text{O}_{6.51}$. Full and empty symbols stand for data taken along the $(0,1,0)$ and $(1,0,0)$ directions, respectively.

C. Temperature dependence

The temperature dependence of the CDW peak intensity is plotted in Fig. 8 for representative samples. In agreement with prior work, we note that the intensity is maximal around T_c in all samples except the one with $x = 0.86$, where the maximum appears to be slightly below T_c . The superconductivity-induced intensity reduction is most pronounced for $p \sim 0.12$, and it is less marked

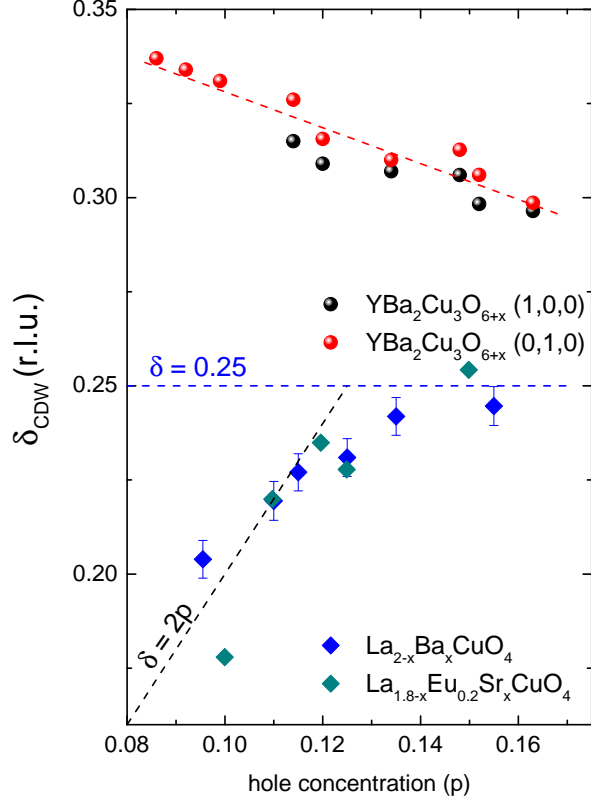


FIG. 6: (Color online) Doping dependence of the CDW wavevector in $\text{YBa}_2\text{Cu}_3\text{O}_{6+x}$ compared to the wave vector characterizing charge order in the “striped” state of $\text{La}_{2-x}\text{Ba}_x\text{CuO}_4$ (Ref. 6) and $\text{La}_{1.8-x}\text{Eu}_{0.2}\text{Ba}_x\text{CuO}_4$ (Ref. 5).

near the end points of the CDW stability range. Fig. 9 shows that the FWHM of the CDW peak follows a related trend. The peaks first become narrower upon cooling from high temperature, indicating progressive expansion of the CDW correlation volume, and then broaden again below T_c , reflecting the suppression of CDW order by superconductivity. Once again, this behavior is most pronounced for $p \sim 0.12$.

Figure 10 shows the doping dependence of the onset temperature of the CDW signal, T_{CDW} , which depends non-monotonically on p . The maximum of the $T_{CDW}(p)$ “dome” coincides with the maxima in the CDW amplitude (Figs. 3 and 4) and correlation length (Fig. 5).

D. Magnetic field dependence

Previous hard x-ray studies reported a large enhancement of the CDW peak intensity in magnetic fields up to 17 T^{26,27}. In the present study, the maximal magnetic field is limited to 6 T, which was already enough to observe an enhancement of the integrated intensity of the CDW peak by a factor ~ 2 in our $\text{YBCO}_{6.55}$ single crys-

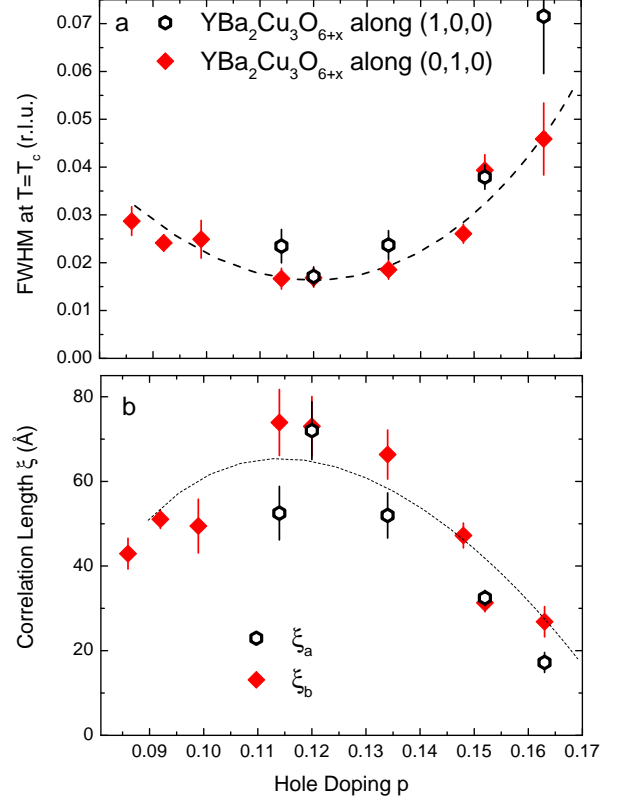


FIG. 7: (Color online) a) CDW peak full-width-at-half-maximum (FWHM) as function of doping, given in reciprocal lattice units (r.l.u.) and measured at $T = T_c$ in our $\text{YBa}_2\text{Cu}_3\text{O}_{6+x}$ samples. b) Corresponding correlation length, defined as $\xi_{a,b} = \frac{a,b}{\pi \times \text{FWHM}}$. Dashed lines are guides to the eyes.

tal²⁴. In Fig. 11, we show analogous measurements performed on the $\text{YBCO}_{6.55}$, $\text{YBCO}_{6.48}$ and $\text{YBCO}_{6.45}$ crystals, with and without applied magnetic field at $T = 4$ K. In agreement with our previous study, an enhancement of the CDW peak intensity by a factor of ~ 2 is seen when applying a field of 6 T to the $\text{YBCO}_{6.55}$ sample. This magnetic-field induced enhancement of the CDW peak is however strongly reduced at lower p , and in $\text{YBCO}_{6.45}$, the effect of the field on the amplitude and width of the CDW peak is no longer discernible. The H -dependence of the integrated intensity in all three samples is summarized in Fig. 12.

The magnetic field induced enhancement of the CDW peak seen in $\text{YBCO}_{6.55}$ confirms the competition between the CDW and superconductivity already apparent in Fig. 8. Due to this competition, CDW correlations are diminished in the superconducting state, but are restored when the field weakens superconductivity. The weaker field dependence observed in $\text{YBCO}_{6.48}$ and $\text{YBCO}_{6.45}$ is presumably a consequence of the competition with yet another phase, incommensurate magnetic order, which becomes the leading instability for

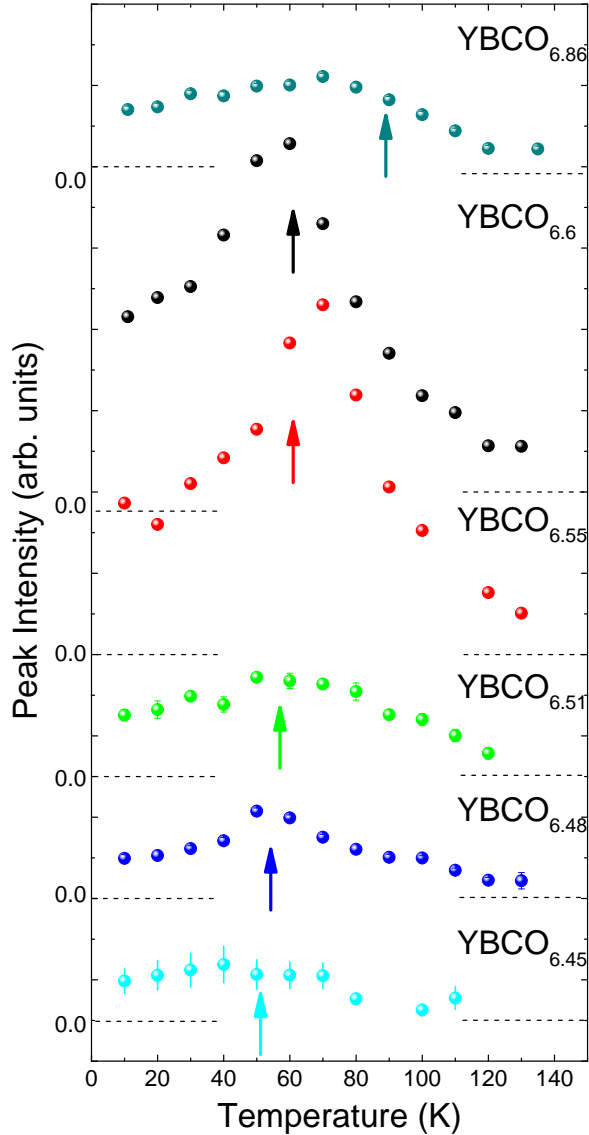


FIG. 8: (Color online) Temperature dependence of the CDW peak intensity for a set of $\text{YBa}_2\text{Cu}_3\text{O}_{6+x}$ samples with $0.44 < x < 0.86$ along the (0,1,0) direction. The plots have been shifted vertically for clarity, and the arrows correspond to the superconducting T_c .

$p < p_{c1}$ ⁷¹. Indeed, prior neutron scattering data have demonstrated a magnetic field induced enhancement of incommensurate spin density wave (SDW) order for a $\text{YBCO}_{6.45}$ sample,⁴⁹ which mirrors the behavior of the CDW for $\text{YBCO}_{6.55}$ seen in Fig. 12. This conclusion is supported by the fact that the linewidths of the CDW reflections in $\text{YBCO}_{6.48}$ and $\text{YBCO}_{6.45}$ remain unaffected by the magnetic field, unlike the behavior for more highly doped samples (Fig. 12). The data presented here thus support the three-phase competition for $p \sim p_{c1}$ inferred from prior work²⁴. The effect of magnetic fields for higher

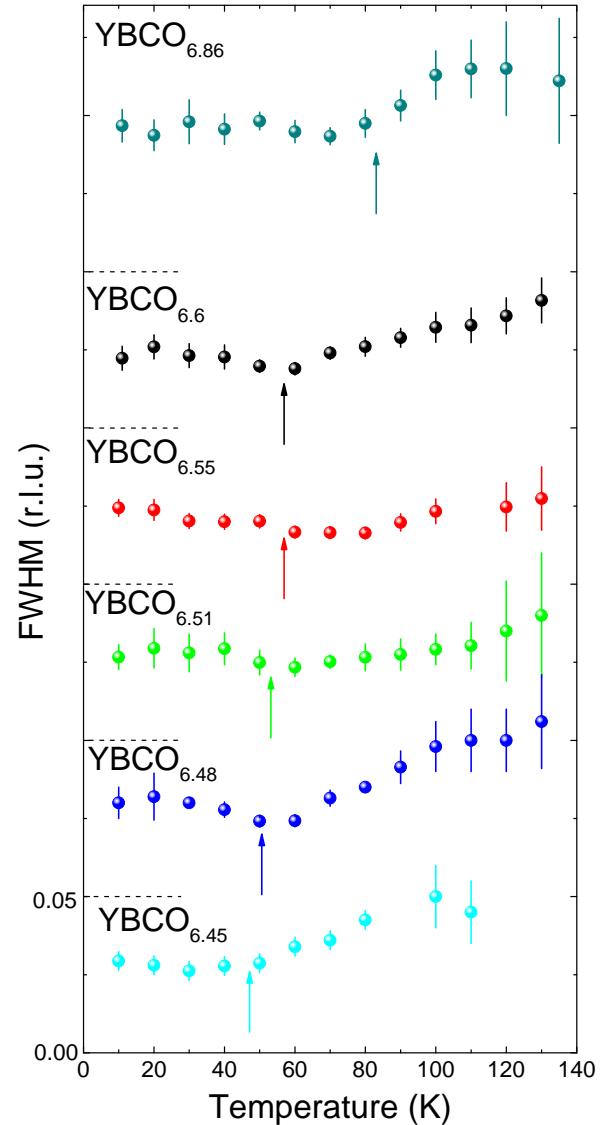


FIG. 9: (Color online) Temperature dependence of the CDW peak FWHM for a set of $\text{YBa}_2\text{Cu}_3\text{O}_{6+x}$ samples with $0.44 < x < 0.86$ along the (0,1,0) direction. The plots have been shifted vertically for clarity, and the arrows correspond to the superconducting T_c .

p has not been investigated here. Since the critical field for superconductivity is much larger around optimal doping, we do not expect any significant field effect on the CDW in the 6 T field available for this study.

IV. DISCUSSION

We now discuss the relationship of our observations to other prominent phenomena in the underdoped cuprates. Our discussion will remain on a phenomenological level, and we will refer to the rapidly evolving theoretical liter-

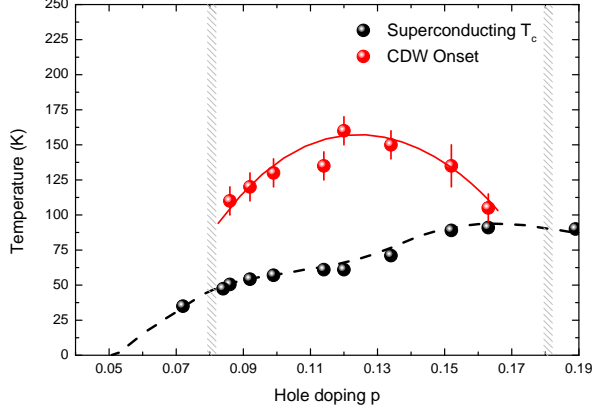


FIG. 10: (Color online) Doping dependence of the onset temperature of the CDW in $\text{YBa}_2\text{Cu}_3\text{O}_{6+x}$. The point at $p \sim 0.13$ has been taken from Ref. 23.

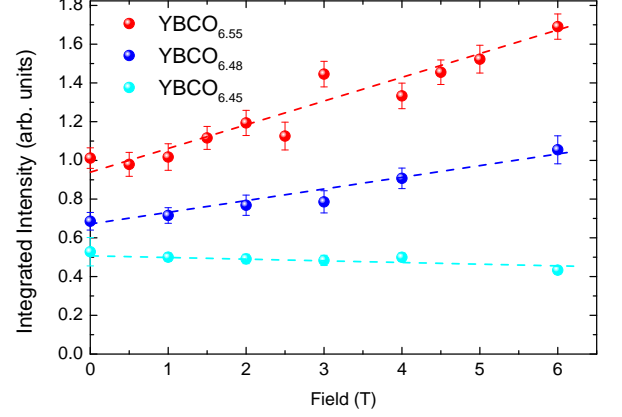


FIG. 12: Magnetic field dependence of the integrated intensity of the RXS reflections in $\text{YBa}_2\text{Cu}_3\text{O}_{6.55}$, $\text{YBa}_2\text{Cu}_3\text{O}_{6.48}$, and $\text{YBa}_2\text{Cu}_3\text{O}_{6.45}$. Dashed lines are guides to the eye.

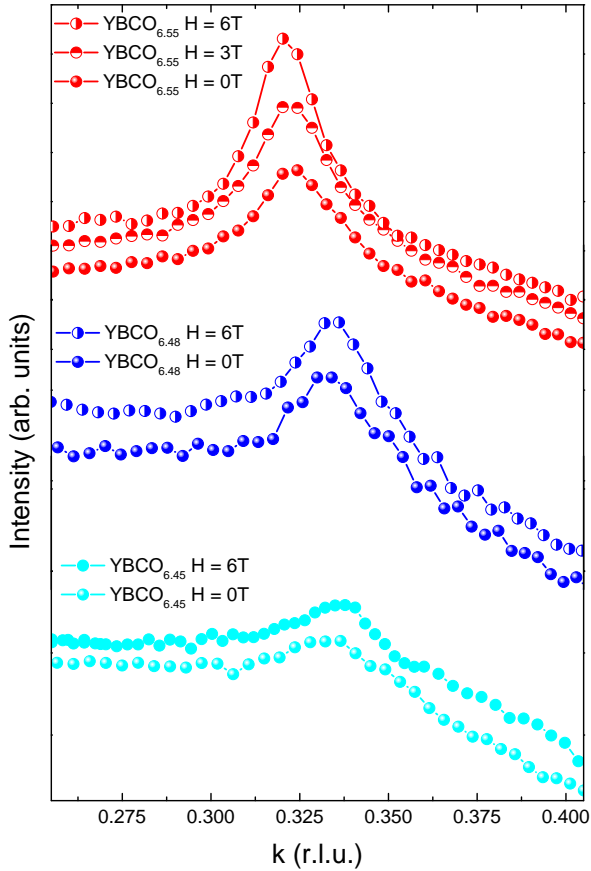


FIG. 11: (Color online) a) Comparison of the RXS data for $\text{YBa}_2\text{Cu}_3\text{O}_{6+x}$, with $x = 0.45, 0.48$, and 0.55 for magnetic fields $H = 0$ and 6 T at $T = 4$ K. A vertical offset has been applied for clarity.

ature for information about the different theoretical approaches to these issues.

A. CDW quantum critical points

Based on accurate RXS data on high-quality single crystals, we have detected CDW order in YBCO_{6+x} for $p_{c1} \leq p \leq p_{c2}$ with $p_{c1} \sim 0.08$ and $p_{c2} \sim 0.18$. The critical divergence of the CDW fluctuations upon cooling is abruptly cut off below the superconducting transition temperature (Fig. 8), so that the CDW does not exhibit genuine long-range order at any point in the phase diagram investigated in this study. The points $p_{c1}, T = 0$ and $p_{c2}, T = 0$ in the two-dimensional phase diagram shown in Fig. 10 should therefore not be regarded as genuine quantum critical points. Recent transport experiments in high external magnetic fields suggest that they may instead be end points of crossover lines connected to proximate zero-temperature critical points in a three-dimensional phase diagram where the field acts as a control parameter.^{59,60}

The magnetic field weakens superconductivity and extend the critical divergence of the CDW correlations to lower temperatures (Fig. 11). The transport experiments indicate that this trend continues in higher fields, and that a “naked” CDW quantum critical point can be exposed in sufficiently large H . p_{c1} is very close to the doping level at which quantum oscillation data have revealed an electron mass divergence pointing to a quantum critical point associated with the metal-to-insulator transition⁵⁷. Evidence has also been reported for a Lifshitz transition of the Fermi surface⁵⁸ and a maximum of the critical field for superconducting long-range order⁵⁹ for $p \sim p_{c1}$. However, the phase behavior near p_{c1} is complicated by the three-phase competition between CDW,

SDW, and superconductivity, whose p - and H -evolution requires further study.

The behavior near the critical doping level p_{c2} suggested by the data presented here is not affected by competition with a third phase. Recent high-field quantum oscillation data indicate an electron mass divergence for $p \rightarrow p_{c2}$ that mirrors the behavior near p_{c1} and suggests that the doping-induced disappearance of the CDW is indeed associated with quantum criticality.⁶⁰ Remarkably, p_{c2} is close to the doping level at which the superconducting transition temperature is maximum for $H = 0$.

B. Relation to the pseudogap and superconducting fluctuations

For the discussion of the phase diagram at nonzero T , it is important to note that the CDW onset temperature $T_{CDW}(p)$ (Fig. 10) is not a thermodynamic phase boundary. Non-resonant x-ray scattering experiments with high energy resolution²⁹ as well as NMR experiments⁶¹ rather indicate that it corresponds to the onset of static CDW short-range order nucleated by residual defects, which are present even in the highest-quality single crystals. However, the coincident maxima of the CDW onset temperature (Fig. 10), amplitude (Figure 4), and correlation length (Fig. 9) at the same doping level, $p \sim 0.12$, indicate an maximum in the intrinsic strength of the CDW, independent of the nature and propensity of defects in the 123 structure. Further evidence for this line of reasoning comes from investigations of the 214 compounds, where a maximum is observed around the same doping level.⁶

Based on these considerations, we now address the relationship of the CDW and the pseudogap, another generic feature of the underdoped cuprates. Although the the pseudogap onset temperature line $T^*(p)$ is still subject of debate, evidence from a variety of thermodynamic and spectroscopic probes suggest that it ends inside the superconducting dome, at a doping level that coincides with the end point of the CDW stability range, $p_{c2} \sim 0.18$, determined in the present study.⁶² Since the “Fermi arc” phenomenon is intimately tied to the pseudogap, this observation is consistent with the “Fermi arc nesting” scenario for CDW formation proposed by Comin *et al.*³². For $p < p_{c2}$, both $T_{CDW}(p)$ (Fig. 10) and $T^*(p)$ increase with decreasing p , again in agreement with this scenario. As noted earlier³¹, $T_{CDW}(p)$ always remains below $T^*(p)$ and goes through a maximum at $p \sim 0.12$, whereas $T^*(p)$ increases monotonically with decreasing p . This confirms that the CDW correlations are not the root cause of the pseudogap phenomenon, and that at least for low to moderate doping the pseudogap cannot be thought of as a CDW gap.⁶³ Rather, the CDW must be regarded as an instability inside the pseudogap regime. We also point out that the temperature dependence of the CDW correlations reported here does not track the one of the polar Kerr effect^{64,65} and the $q = 0$ magnetic order

detected by neutron diffraction^{66–68}, leaving open at this stage the relationship between the CDW fluctuations and these effects⁶⁹.

On the other hand, it is interesting to note the close similarity of $T_{CDW}(p)$ and the onset of intra-bilayer superconducting fluctuations in YBCO_{6+x} inferred from the c -axis optical conductivity, which also exhibits a dome-like shape in the $p - T$ diagram, with a shallow peak for $p \sim 0.1$ and $T \sim 180$ K.⁷⁰ The combined onset of superconducting and CDW fluctuations and the wide fluctuation regime suggest a composite order parameter subject to strong phase fluctuations, consistent with recent proposals of a fluctuating pair density wave (PDW) state.^{71–78} While d -wave superconductivity preempts PDW long-range order for $H = 0$, recent magnetometric experiments suggest that it may be the leading instability in high magnetic fields.⁷⁹

C. In-plane anisotropy and relationship to stripes

The in-plane anisotropy provides further information about the microscopic structure of the CDW state. We have shown that this quantity evolves systematically as a function of doping (Fig. 5). For $p \sim 0.12$, where the intensity, correlation length, and onset temperature of the CDW correlations are maximal, the RXS peaks along the H - and K -directions have approximately the same amplitude. This is most easily understood in terms of a biaxial “checkerboard” modulation, although an accidental, approximately equal mixture of uniaxial domains cannot be ruled out based on the data presented here. Away from this doping level, the in-plane anisotropy increases. For $p \rightarrow p_{c1}$, the peak along h disappears below the detection limit, consistent with a uniaxial modulation. For $p \rightarrow p_{c2}$, on the other hand, the RXS peaks along k become more intense.

One might be tempted to associate the in-plane anisotropy of the CDW and its p -evolution with changes in the electronic structure induced by the commensurate ordering of oxygen dopant atoms in the chain layer. In this case, however, one would expect that the degradation of ortho-II order for $x < 0.5$ restores the isotropy of the CDW peaks, which is clearly not the case. Indeed, the anisotropy persists down to the lowest doping level where the CDW is observed. The apparent p -induced sign reversal of the intensity anisotropy is also difficult to attribute to oxygen order in the chains. While an influence of the ortho-I structure on the modest anisotropy at high p cannot be ruled out, the large anisotropy for $p \rightarrow p_{c1}$ appears to be a consequence of an intrinsic tendency towards uniaxial CDW order in the CuO_2 planes. A related trend is observed in the spin fluctuation spectrum as p_{c1} is approached from below.⁴⁸ Note, however, that the propagation vector of the incommensurate spin fluctuation is along h , that is, perpendicular to the soft charge fluctuations for $p > p_{c1}$.

Unless the isotropy of the CDW for $p \sim 0.12$ is purely

accidental, it thus appears that the fluctuations in the center of the CDW “dome” (Fig. 10) are biaxial, whereas those for both lower and higher doping are increasingly uniaxial. Qualitatively, this situation resembles the recently investigated phase diagram of helical magnets in magnetic fields, which include both single- q (spiral) and multiple- q (skyrmion lattice) states.^{80,81} In the cuprates, the distinction between single- and double- q CDW structures is possibly blurred by disorder. We note, however, that sound velocity measurements performed on a ortho-II ordered YBCO_{6.55} single crystal under large magnetic field indicate a biaxial modulation³⁰. Moreover, according to model calculations only a biaxial modulation can induce a Fermi surface reconstruction compatible with the experimentally observed period of the quantum oscillations⁴¹. Surprisingly, quantum oscillations have been reported at high magnetic fields even in the regime $0.086 \leq p \leq 0.1$ where our low-field data indicate uniaxial CDW order (Fig. 5), with no qualitative differences to the regime with more isotropic CDW correlations at higher p . At this stage, it cannot be excluded that the long-range ordered CDW state for high H differs from the short-range ordered state at lower H . Julien *et al.* have suggested that a transition between two CDW states occurs at $H \sim 20$ T.⁶¹ At the present time, this field is difficult to access with scattering probes.

We now discuss in more detail the relationship between the charge modulations we have described in the 123 system to those in the 214 system, which have been widely discussed in terms of uniaxial (“stripe”) modulations. We have already noted that the momentum-integrated amplitudes of the CDW peaks in both materials are comparable²⁵. Comparison between our current measurements and prior RXS work on La_{2- x} Ba _{x} CuO₄ (Ref. 6) and La_{1.8- x} Eu_{0.2}Ba _{x} CuO₄ (Ref. 5) now shows that the CDW stability ranges (Fig. 4) are also remarkably similar in the 123 and 214 system, as are the pronounced maxima of the amplitude, correlation length, and onset temperature of the charge-ordering reflections for $p \sim 0.12$. In both cases, the superconducting T_c is reduced in this range of doping levels, at least with respect to the quadratic T_c -versus- p relation that can be extrapolated from lower and higher p ⁸². Finally, we note that there is a striking analogy between the anomalies in the phonon dispersions^{83,84} and transport properties^{42,57} associated with the charge modulations in both families of compounds.

On the other hand, the charge correlations in the 123 and 214 also exhibit quantitative and qualitative differences. The most striking difference is the opposite doping dependence of δ_{CDW} in the two families (Fig. 4). In 214 compounds⁴⁻⁶, it is well established that the wave vector of the charge modulation increases with doping (Fig. 6), in lockstep with the p -dependence of the spin correlations with incommensurability $\delta_{SDW} = \delta_{CDW}/2$,⁵⁰ and then saturates near the commensurate value $\delta_{CDW} = 1/4$. In the 123 system, the wave vector characterizing the quasi-static, nearly antiferromagnetic spin correlations close to

the Mott-insulating state ($p \lesssim 0.08$) also increases with increasing doping.⁴⁸ Since a similar trend has recently been established for the nearly critical spin fluctuations in Bi₂Sr₂CuO_{6+ δ} at low p ,⁸⁵ this behavior can be regarded as universal for the deeply underdoped regime of the cuprate phase diagram.

Whereas coupled, nearly critical spin and charge fluctuations persist in the 214 over a wide range of p , continuing the trend that can be traced back to the Mott-insulator, the 123 system goes through a sharply defined critical point that separates regimes with ungapped ($p < p_{c1}$)⁴⁸ and gapped ($p > p_{c1}$)⁴⁷ spin fluctuations. For $p > p_{c1}$, nearly critical charge fluctuations appear at a wavevector that is tied to the evolution of the Fermi surface^{32,45}. This behavior is also observed for the Bi- and Hg-based cuprates, and can hence be regarded as generic for the moderately doped cuprates. The non-generic behavior in the 214 system (including the apparent lock-in of the CDW wavevector to the commensurate value of $1/4$ for $p \sim 1/8$) may be a consequence of tilt distortions of the CuO₆ octahedra in the 214 lattice structure, which affect the geometry of the Fermi surface. Octahedral tilt patterns of this kind are not observed in other cuprate families. Disorder due to the randomly placed Sr donors may also contribute to the anomalous stability of incommensurate magnetism in the 214 system. Indeed, nonmagnetic impurities were shown to close the spin gap in moderately doped 123, and to induce incommensurate magnetic order at the expense of CDW correlations.^{24,86,87}

V. CONCLUSION

We have detected incommensurate charge density wave fluctuations in YBCO_{6+ x} for hole doping levels $p_{c1} \leq p \leq p_{c2}$ with $p_{c1} \sim 0.08$ and $p_{c2} \sim 0.18$. The onset temperature of the CDW correlations forms a “dome” ranging from p_{c1} to p_{c2} in the $p - T$ phase diagram, with a peak of $T_{CDW} \sim 160$ K for $p \sim 0.12$. The peak temperature coincides with the onset of superconducting fluctuations detected by infrared spectroscopy,⁷⁰ and with the mean-field transition temperature for d -wave superconductivity calculated based on the experimentally observed spin fluctuation spectrum^{88,89}. These findings suggest strong, combined fluctuations of the d -wave superconducting and CDW order parameters, and they are consistent with proposals of a proximate ground state with a composite order parameter (such as the pair density wave) that competes with the uniform d -wave pairing state and generates the plateau in the T_c -versus- p relation.^{38,72-78} Further work is required to establish whether such a state becomes thermodynamically stable in high magnetic fields.

The temperature and magnetic field dependence of the RXS intensity for fixed p , combined with recent high-field transport experiments, suggest proximate CDW quantum critical points for $p = p_{c1}$ and p_{c2} . For $p \lesssim p_{c1}$, soft

incommensurate spin fluctuations set in, and T_c is further reduced, consistent with spin fluctuation mediated pairing models.^{88,89} The presence of similar, ungapped spin fluctuations over a wide doping range may be responsible for the lower maximal T_c in the 214 system. Remarkably, p_{c2} coincides with the doping level optimal for superconductivity, and according to an influential study,⁶² with the end point of the pseudogap regime inside the superconducting dome. In high fields, superconductivity is suppressed most strongly for $p \sim 0.12$, and p_{c1} and p_{c2} become centers of separate superconducting domes. The possible role of quantum-critical CDW fluctuations for the mechanism of high- T_c superconductivity suggested

by these observations is an important subject of future experimental and theoretical research.

Note added. Hücker *et al.* have recently reported similar results on the doping dependence of the CDW in YBCO using hard x-rays diffraction.⁹⁰

Acknowledgements

We acknowledge M.-H. Julien, B. Ramshaw and S. Sebastian for fruitful discussions and sharing with us unpublished data, C.T. Lin for sample preparation.

-
- * Electronic address: b.keimer@fkf.mpg.de
† Electronic address: m.letacon@fkf.mpg.de
- ¹ P. A. Lee, N. Nagaosa, and X. G. Wen, *Review of Modern Physics* **78**, 17 (2006).
 - ² T. Timusk and B. W. Statt, *Reports on Progress in Physics* **62**, 61 (1999).
 - ³ J. M. Tranquada, B. J. Sternlieb, J. D. Axe, Y. Nakamura, and S. Uchida, *Nature* **375**, 561 (1995).
 - ⁴ J. Fink, E. Schierle, E. Weschke, J. Geck, D. Hawthorn, V. Soltwisch, H. Wadati, H.-H. Wu, H. A. Dürr, N. Wizen, B. Büchner, and G. A. Sawatzky, *Phys. Rev. B* **79**, 100502 (2009).
 - ⁵ J. Fink, V. Soltwisch, J. Geck, E. Schierle, E. Weschke, and B. Büchner, *Phys. Rev. B* **83**, 092503 (2011). Kim, *Nature*, **466**, 347, (2010).
 - ⁶ M. Hücker, M. v. Zimmermann, G. D. Gu, Z. J. Xu, J. S. Wen, G. Xu, H. J. Kang, A. Zheludev, and J. M. Tranquada, *Phys. Rev. B* **83**, 104506 (2011).
 - ⁷ M. Hücker, M. v. Zimmermann, Z. J. Xu, J. S. Wen, G. D. Gu, and J. M. Tranquada, *Phys. Rev. B* **87**, 014501 (2013).
 - ⁸ S. B. Wilkins, M. P. M. Dean, J. o. r. Fink, M. Hücker, J. Geck, V. Soltwisch, E. Schierle, E. Weschke, G. Gu, S. Uchida, N. Ichikawa, J. M. Tranquada, and J. P. Hill, *Phys. Rev. B* **84**, 195101 (2011).
 - ⁹ S. A. Kivelson, I. P. Bindloss, E. Fradkin, V. Oganessian, J. M. Tranquada, A. Kapitulnik, and C. Howald, *Reviews of Modern Physics* **75**, 1201 (2003).
 - ¹⁰ M. Vershinin, S. Misra, S. Ono, Y. Abe, Y. Ando, and A. Yazdani, *Science* **303**, 1995 (2004).
 - ¹¹ P. Abbamonte, A. Rusydi, S. Smadici, G. D. Gu, G. A. Sawatzky, and D. L. Feng, *Nat. Phys.* **1**, 155 (2005).
 - ¹² Y. Kohsaka, C. Taylor, K. Fujita, A. Schmidt, C. Lupien, T. Hanaguri, M. Azuma, M. Takano, H. Eisaki, H. Takagi, S. Uchida, and J. C. Davis, *Science* **315**, 1380 (2007).
 - ¹³ B. Muschler, W. Prestel, L. Tassini, R. Hackl, M. Lambacher, A. Erb, S. Komiyama, Y. Ando, D. C. Peets, W. N. Hardy, R. Liang, and D. A. Bonn, *The European Physical Journal - Special Topics* **188**, 131 (2010).
 - ¹⁴ J. E. Hoffman, E. W. Hudson, K. M. Lang, V. Madhavan, H. Eisaki, S. Uchida, and J. C. Davis, *Science* **295**, 466 (2002).
 - ¹⁵ T. Hanaguri, C. Lupien, Y. Kohsaka, D. H. Lee, M. Azuma, M. Takano, H. Takagi, and J. C. Davis, *Nature* **430**, 1001 (2004).
 - ¹⁶ W. D. Wise, M. C. Boyer, K. Chatterjee, T. Kondo, T. Takeuchi, H. Ikuta, Y. Wang, and E. W. Hudson, *Nat. Phys.* **4**, 696 (2008).
 - ¹⁷ J.-H. Ma, Z.-H. Pan, F. C. Niestemski, M. Neupane, Y.-M. Xu, P. Richard, K. Nakayama, T. Sato, T. Takahashi, H.-Q. Luo, L. Fang, H.-H. Wen, Ziqiang Wang, H. Ding, and V. Madhavan, *Phys. Rev. Lett.* **101**, 207002 (2008).
 - ¹⁸ C. V. Parker, P. Aynajian, E. H. da Silva Neto, A. Pushp, S. Ono, J. Wen, Z. Xu, G. Gu, and A. Yazdani, *Nature* **468**, 677 (2010).
 - ¹⁹ M. J. Lawler, K. Fujita, Jinhwan Lee, A. R. Schmidt, Y. Kohsaka, C. K. Kim, H. Eisaki, S. Uchida, J. C. Davis, J. P. Sethna, and Eun-Ah Kim, *Nature* **466**, 347-351 (2010).
 - ²⁰ T. Wu, H. Mayaffre, S. Krämer, M. Horvatić, C. Berthier, P. L. Kuhns, A. P. Reyes, R. Liang, W. N. Hardy, D. A. Bonn, and M.-H. Julien, *Nat. Commun.* **4**, (2013).
 - ²¹ T. Wu, H. Mayaffre, S. Krämer, M. Horvatic, C. Berthier, W. N. Hardy, R. Liang, D. A. Bonn, and M.-H. Julien, *Nature* **477**, 191 (2011).
 - ²² G. Ghiringhelli, M. Le Tacon, M. Minola, S. Blanco-Canosa, C. Mazzoli, N. B. Brookes, G. M. De Luca, A. Frano, D. G. Hawthorn, F. He, T. Loew, M. M. Sala, D. C. Peets, M. Salluzzo, E. Schierle, R. Sutarto, G. A. Sawatzky, E. Weschke, B. Keimer, and L. Braicovich, *Science* **337**, 821 (2012).
 - ²³ A. J. Achkar, R. Sutarto, X. Mao, F. He, A. Frano, S. Blanco-Canosa, M. Le Tacon, G. Ghiringhelli, L. Braicovich, M. Minola, M. Moretti Sala, C. Mazzoli, R. Liang, D. A. Bonn, W. N. Hardy, B. Keimer, G. A. Sawatzky, and D. G. Hawthorn, *Phys. Rev. Lett.* **109**, 167001 (2012).
 - ²⁴ S. Blanco-Canosa, A. Frano, T. Loew, Y. Lu, J. Porras, G. Ghiringhelli, M. Minola, C. Mazzoli, L. Braicovich, E. Schierle, E. Weschke, M. Le Tacon, and B. Keimer, *Phys. Rev. Lett.* **110**, 187001 (2013).
 - ²⁵ V. Thampy, S. Blanco-Canosa, M. Garcia-Fernandez, M. P. M. Dean, G. D. Gu, M. Först, T. Loew, B. Keimer, M. Le Tacon, S. B. Wilkins, and J. P. Hill, *Phys. Rev. B* **88**, 024505 (2013).
 - ²⁶ J. Chang, E. Blackburn, A. T. Holmes, N. B. Christensen, J. Larsen, J. Mesot, R. Liang, D. A. Bonn, W. N. Hardy, A. Watenphul, M. v. Zimmermann, E. M. Forgan, and S. M. Hayden, *Nat. Phys.* **8**, 871 (2012).
 - ²⁷ E. Blackburn, J. Chang, M. Hücker, A. T. Holmes, N. B. Christensen, R. Liang, D. A. Bonn, W. N. Hardy, U. Rütt,

- O. Gutowski, M. v. Zimmermann, E. M. Forgan, and S. M. Hayden, *Phys. Rev. Lett.* **110**, 137004 (2013).
- ²⁸ E. Blackburn, J. Chang, A. H. Said, B. M. Leu, R. Liang, D. A. Bonn, W. N. Hardy, E. M. Forgan, and S. M. Hayden, *Phys. Rev. B* **88**, 054506 (2013).
 - ²⁹ M. Le Tacon, A. Bosak, S. M. Souliou, G. Dellea, T. Loew, R. Heid, K. P. Bohnen, G. Ghiringhelli, M. Krisch, and B. Keimer, *Nat. Phys.* **10**, 52 (2014).
 - ³⁰ D. LeBoeuf, S. Kramer, W. N. Hardy, R. Liang, D. A. Bonn, and C. Proust, *Nat. Phys.* **9**, 79 (2013).
 - ³¹ M. Bakr, S. M. Souliou, S. Blanco-Canosa, I. Zegkinoglou, H. Gretarsson, J. Stremper, T. Loew, C. T. Lin, R. Liang, D. A. Bonn, W. N. Hardy, B. Keimer, and M. Le Tacon, *Phys. Rev. B* **88**, 214517 (2013).
 - ³² R. Comin, A. Frano, M. M. Yee, Y. Yoshida, H. Eisaki, E. Schierle, E. Weschke, R. Sutarto, F. He, A. Soumyanarayanan, Y. He, M. Le Tacon, I. S. Elfimov, J. E. Hoffman, G. A. Sawatzky, B. Keimer, and A. Damascelli, *Science* **343**, 390 (2014).
 - ³³ E. H. da Silva Neto, P. Aynajian, A. Frano, R. Comin, E. Schierle, E. Weschke, A. Gyenis, J. Wen, J. Schneeloch, Z. Xu, S. Ono, G. Gu, M. Le Tacon, and A. Yazdani, *Science* **343**, 393 (2014).
 - ³⁴ N. Doiron-Leyraud, S. Lepault, O. Cyr-Choinière, B. Vignolle, G. Grissonnanche, F. Laliberté, J. Chang, N. Barisic, M. K. Chan, L. Ji, X. Zhao, Y. Li, M. Greven, C. Proust, and L. Taillefer, *Physical Review X* **3**, 021019 (2013).
 - ³⁵ S. E. Sebastian, N. Harrison, and G. G. Lonzarich, *Reports on Progress in Physics* **75**, 102501 (2012).
 - ³⁶ N. Doiron-Leyraud, C. Proust, D. LeBoeuf, J. Levallois, J.-B. Bonnemaïson, R. Liang, D. A. Bonn, W. N. Hardy, and L. Taillefer, *Nature* **447**, 566 (2007).
 - ³⁷ J. Zaanen and O. Gunnarsson, *Phys. Rev. B* **40**, 7391 (1989).
 - ³⁸ M. Vojta, *Advances in Physics* **58**, 699 (2009).
 - ³⁹ J. Bobroff, H. Alloul, S. Ouazi, P. Mendels, A. Mahajan, N. Blanchard, G. Collin, V. Guillen, and J. F. Marucco, *Phys. Rev. Lett.* **89**, 157002 (2002).
 - ⁴⁰ M. v. Zimmermann, J. R. Schneider, T. Frello, N. H. Andersen, J. Madsen, M. Käll, H. F. Poulsen, R. Liang, P. Dosanjh, and W. N. Hardy, *Phys. Rev. B* **68**, 104515 (2003).
 - ⁴¹ S. E. Sebastian, N. Harrison, R. Liang, D. A. Bonn, W. N. Hardy, C. H. Mielke, and G. G. Lonzarich, *Phys. Rev. Lett.* **108**, 196403 (2012).
 - ⁴² F. Laliberté, J. Chang, N. Doiron-Leyraud, E. Hassinger, R. Daou, M. Rondeau, B. J. Ramshaw, R. Liang, D. A. Bonn, W. N. Hardy, S. Pyon, T. Takayama, H. Takagi, I. Sheikin, L. Malone, C. Proust, K. Behnia, and L. Taillefer, *Nat. Commun.* **2**, 432 (2011).
 - ⁴³ A. F. Bangura, J. D. Fletcher, A. Carrington, J. Levallois, M. Nardone, B. Vignolle, P. J. Heard, N. Doiron-Leyraud, D. LeBoeuf, L. Taillefer, S. Adachi, C. Proust, and N. E. Hussey, *Phys. Rev. Lett.* **100**, 047004 (2008).
 - ⁴⁴ N. Harrison and S. E. Sebastian, *Phys. Rev. Lett.* **106**, 226402 (2011).
 - ⁴⁵ W. Tabis, Y. Li, M. Le Tacon, L. Braicovich, A. Kreyssig, M. Minola, G. Dellea, E. Weschke, M. J. Veit, M. Ramazanoglu, A. I. Goldman, T. Schmitt, G. Ghiringhelli, N. Barišić, M. K. Chan, C. J. Dorow, G. Yu, X. Zhao, B. Keimer, and M. Greven, <http://arxiv.org/abs/1404.7658>.
 - ⁴⁶ P. Dai, H. A. Mook, S. M. Hayden, G. Aeppli, T. G. Perring, R. D. Hunt, and F. Dogan, *Science* **284**, 1344 (1999).
 - ⁴⁷ H. F. Fong, P. Bourges, Y. Sidis, L. P. Regnault, J. Bossy, A. Ivanov, D. L. Milius, I. A. Aksay, and B. Keimer, *Phys. Rev. B* **61**, 14773 (2000).
 - ⁴⁸ D. Haug, V. Hinkov, Y. Sidis, P. Bourges, N. B. Christensen, A. Ivanov, T. Keller, C. T. Lin, and B. Keimer, *New J. Phys.* **12**, 105006 (2010).
 - ⁴⁹ D. Haug, V. Hinkov, A. Suchaneck, D. S. Inosov, N. B. Christensen, C. Niedermayer, P. Bourges, Y. Sidis, J. T. Park, A. Ivanov, C. T. Lin, J. Mesot, and B. Keimer, *Phys. Rev. Lett.* **103**, (2009).
 - ⁵⁰ M. Fujita, H. Hiraka, M. Matsuda, M. Matsuura, J. M. Tranquada, S. Wakimoto, G. Y. Xu, and K. Yamada, *Journ. Phys. Soc. Jap.* **81**, (2012).
 - ⁵¹ V. Hinkov, S. Pailhès, P. Bourges, Y. Sidis, A. Ivanov, A. Kulakov, C. T. Lin, D. P. Chen, C. Bernhard, B. Keimer, *Nature* **430**, 650 (2004).
 - ⁵² T. B. Lindemer, J. F. Hunley, J. E. Gates, A. L. Sutton, J. Brynestad, C. R. Hubbard, and P. K. Gallagher, *J. Amer. Ceram. Soc.* **72**, 1775 (1989).
 - ⁵³ R. Liang, D. A. Bonn, and W. N. Hardy, *Phys. Rev. B* **73**, 180505 (2006).
 - ⁵⁴ J. Stremper, I. Zegkinoglou, U. Rütt, M. v. Zimmermann, C. Bernhard, C. T. Lin, T. Wolf, and B. Keimer, *Phys. Rev. Lett.* **93**, 157007 (2004).
 - ⁵⁵ J. Fink, E. Schierle, E. Weschke, and J. Geck, *Reports on Progress in Physics* **76**, 056502 (2013).
 - ⁵⁶ A. J. Achkar, X. Mao, C. McMahon, R. Sutarto, F. He, R. Liang, D. A. Bonn, W. N. Hardy, and D. G. Hawthorn, <http://arxiv.org/abs/1312.6630>
 - ⁵⁷ S. E. Sebastian, N. Harrison, M. M. Altarawneh, C. H. Mielke, R. Liang, D. A. Bonn, and G. G. Lonzarich, *Proceedings of the National Academy of Sciences* **107**, 6175 (2010).
 - ⁵⁸ D. LeBoeuf, N. Doiron-Leyraud, B. Vignolle, M. Sutherland, B. J. Ramshaw, J. Levallois, R. Daou, F. Laliberté, O. Cyr-Choinière, J. Chang, Y. J. Jo, L. Balicas, R. Liang, D. A. Bonn, W. N. Hardy, C. Proust, and L. Taillefer, *Phys. Rev. B* **83**, 054506 (2011).
 - ⁵⁹ G. Grissonnanche, O. Cyr-Choinière, F. Laliberté, S. Ren de Cotret, A. Juneau-Fecteau, S. Dufour-Beauséjour, M. E. Delage, D. LeBoeuf, J. Chang, B. J. Ramshaw, D. A. Bonn, W. N. Hardy, R. Liang, S. Adachi, N. E. Hussey, B. Vignolle, C. Proust, M. Sutherland, S. Krämer, J. H. Park, D. Graf, N. Doiron-Leyraud, and L. Taillefer, *Nat. Commun.* **5**, (2014).
 - ⁶⁰ B. Ramshaw, *private communication*
 - ⁶¹ T. Wu, H. Mayaffre, S. Krämer, M. Horvatić, C. Berthier, W. N. Hardy, R. Liang, D. A. Bonn, M.-H. Julien, <http://arxiv.org/abs/1404.1617>.
 - ⁶² J. L. Tallon and J. W. Loram, *Physica C: Superconductivity* **349**, 53 (2001).
 - ⁶³ H. Alloul, *Comptes Rendus Physique, in press* (2014)
 - ⁶⁴ J. Xia, E. Schemm, G. Deutscher, S. A. Kivelson, D. A. Bonn, W. N. Hardy, R. Liang, W. Siemons, G. Koster, M. M. Fejer, and A. Kapitulnik, *Phys. Rev. Lett.* **100**, 127002 (2008).
 - ⁶⁵ A. Kapitulnik, J. Xia, E. Schemm, and A. Palevski, *New J. Phys.* **11**, 055060 (2009).
 - ⁶⁶ Y. Li, V. Balédent, N. Barišić, Y. Cho, B. Fauqué, Y. Sidis, G. Yu, X. Zhao, P. Bourges, and M. Greven, *Nature* **455**, 372 (2008).
 - ⁶⁷ B. Fauqué, Y. Sidis, V. Hinkov, S. Pailhès, C. T. Lin, X. Chaud, and P. Bourges, *Phys. Rev. Lett.* **96**, 197001 (2006).
 - ⁶⁸ V. Balédent, D. Haug, Y. Sidis, V. Hinkov, C. T. Lin, and

- P. Bourges, *Phys. Rev. B* **83**, 104504 (2011).
- ⁶⁹ P. Hosur, A. Kapitulnik, S. A. Kivelson, J. Orenstein, and S. Raghu, *Phys. Rev. B* **87**, 115116 (2013).
- ⁷⁰ A. Dubroka, M. Rössle, K. W. Kim, V. K. Malik, D. Munzar, D. N. Basov, A. A. Schafgans, S. J. Moon, C. T. Lin, D. Haug, V. Hinkov, B. Keimer, T. Wolf, J. G. Storey, J. L. Tallon, and C. Bernhard, *Phys. Rev. Lett.* **106**, 047006 (2011).
- ⁷¹ M.A. Metlitski and S. Sachdev, *New J. Phys.* **12**, 105007 (2010).
- ⁷² K. B. Efetov, H. Meier, and C. Pepin, *Nat. Phys.* **9**, 442 (2013).
- ⁷³ H. Meier, M. Einenkel, C. Pépin, and K. B. Efetov, *Phys. Rev. B* **88**, 020506 (2013).
- ⁷⁴ S. Sachdev and R. La Placa, *Phys. Rev. Lett.* **111**, 027202 (2013).
- ⁷⁵ H. Meier, C. Pépin, M. Einenkel, and K. B. Efetov, *arXiv:1312.2010*.
- ⁷⁶ L. E. Hayward, D. G. Hawthorn, R. G. Melko, and S. Sachdev, *Science* **343**, 1336 (2014).
- ⁷⁷ Y. Wang, A. V. Chubukov, *arXiv:1401.0712*.
- ⁷⁸ L. Nie, G. Tarjus, S. A. Kivelson *arXiv:1311.5580*.
- ⁷⁹ Fan Yu, M. Hirschberger, T. Loew, G. Li, B. J. Lawson, T. Asaba, J. B. Kemper, T. Liang, J. Porras, G. S. Boebinger, J. Singleton, B. Keimer, L. Li, and N. P. Ong, <http://arxiv.org/abs/1402.7371>.
- ⁸⁰ T. Adams, A. Chacon, M. Wagner, A. Bauer, G. Brandl, B. Pedersen, H. Berger, P. Lemmens, and C. Pfleiderer, *Phys. Rev. Lett.* **108**, 237204 (2012).
- ⁸¹ S. Seki, J.-H. Kim, D. S. Inosov, R. Georgii, B. Keimer, S. Ishiwata, and Y. Tokura, *Phys. Rev. B* **85**, 220406(R) (2012).
- ⁸² J. L. Tallon, C. Bernhard, H. Shaked, R. L. Hitterman, and J. D. Jorgensen, *Phys. Rev. B* **51**, 12911 (1995).
- ⁸³ D. Reznik, L. Pintschovius, M. Ito, S. Iikubo, M. Sato, H. Goka, M. Fujita, K. Yamada, G. D. Gu, and J. M. Tranquada, *Nature* **440**, 1170 (2006).
- ⁸⁴ M. Raichle, D. Reznik, D. Lamago, R. Heid, Y. Li, M. Bakr, C. Ulrich, V. Hinkov, K. Hradil, C. T. Lin, and B. Keimer, *Phys. Rev. Lett.* **107**, 177004 (2011).
- ⁸⁵ M. Enoki, M. Fujita, T. Nishizaki, S. Iikubo, D. K. Singh, S. Chang, J. M. Tranquada, and K. Yamada, *Phys. Rev. Lett.* **110**, 017004 (2013).
- ⁸⁶ A. Suchaneck, V. Hinkov, D. Haug, L. Schulz, C. Bernhard, A. Ivanov, K. Hradil, C. Lin, P. Bourges, B. Keimer, and Y. Sidis, *Phys. Rev. Lett.* **105**, 037207 (2010).
- ⁸⁷ H. Alloul, J. Bobroff, M. Gabay, and P. J. Hirschfeld, *Reviews of Modern Physics* **81**, 45 (2009).
- ⁸⁸ T. Dahm, V. Hinkov, S. V. Borisenko, A. A. Kordyuk, V. B. Zabolotnyy, J. Fink, B. Buchner, D. J. Scalapino, W. Hanke, and B. Keimer, *Nat. Phys.* **5**, 217 (2009).
- ⁸⁹ M. Le Tacon, G. Ghiringhelli, J. Chaloupka, M. M. Sala, V. Hinkov, M. W. Haverkort, M. Minola, M. Bakr, K. J. Zhou, S. Blanco-Canosa, C. Monney, Y. T. Song, G. L. Sun, C. T. Lin, G. M. De Luca, M. Salluzzo, G. Khaliullin, T. Schmitt, L. Braicovich, and B. Keimer, *Nat. Phys.* **7**, 725 (2011).
- ⁹⁰ M. Hücker, N. B. Christensen, A. T. Holmes, E. Blackburn, E. M. Forgan, Ruixing Liang, D. A. Bonn, W. N. Hardy, O. Gutowski, M. v. Zimmermann, S. M. Hayden, and J. Chang, *arxiv:1405.7001*.